A triazatruxene-based molecular dyad for single-component organic solar cells

Antoine Labrunie [a], Giacomo Londi [b], Sergey V. Dayneko [c], Martin Blais [a], Sylvie Dabos-Seignon [a], Gregory C. Welch [c], David Beljonne [b], Philippe Blanchard [a,*], Clément Cabanetos [a,*]

Email(s): philippe.blanchard@univ-angers.fr; clement.cabanetos@univ-angers.fr

[a] CNRS UMR 6200, MOLTECH-Anjou, University of Angers, 2 Bd Lavoisier, 49045 Angers, France
[b] Chimie des Matériaux Nouveaux & Centre d'Innovation et de Recherche en Matériaux Polymères, Université de Mons - UMONS / Materia Nova, Place du Parc, 20, B-7000 MONS
[c] Department of Chemistry, University of Calgary, 2500 University Drive N.W., Calgary, Alberta T2N 1N4, Canada

Abstract: The synthesis, characterization and use of a new donor-acceptor molecular dyad in single component organic solar cells are reported. The dyad, composed of a triazatruxene-based push-pull 'donor' unit linked to a C_{60} 'acceptor' unit through a non-conjugated σ connector, led to promising power conversion efficiencies of 0.6% when embedded in simple devices exhibiting the architecture: indium tin oxide (ITO)/poly(3,4-ethylenedioxythiophene): polystyrene sulfonic acid (PEDOT:PSS)/dyad/Al.

Keywords: Single component organic solar cells, triazatruxene, dyad, fullerene, organic synthesis, click chemistry.

I. Introduction

With power conversion efficiency (PCE) now exceeding 15% for tandem architectures [1, 2] and 13% for single layers [3], organic photovoltaics (OPV) continues to demonstrate their potential as a viable renewable energy conversion technology [4]. To reach such high efficiencies, efforts have been devoted to controlling the nano-morphology of the bulk heterojunction active layer, usually composed of an electron donor (D) blended with an electron acceptor (A), *via* chemical and device-processing engineering [5-7]. Hence, to improve free charge-carrier generation and transport, several empirical parameters such as the donor/acceptor (D/A) ratio, the nature of the processing solvent, different annealing conditions, and/or the use of additives are routinely assessed and adjusted [8, 9]. However, even if the optimized morphology is luckily achieved, the latter usually evolves leading, in general, to a drastic decrease in the device performance.

In this context, the concept of single-component organic solar cells (SCOSCs) was introduced in the late 90's in which the active layer is solely based on an "all-in-one" molecule built by connecting the donor and the acceptor through a covalent linkage [10,11]. Designed to ensure efficient charge separation, simplified device fabrication and a stable phase segregation, such molecular architectures are generally and unfortunately impeded by high carrier recombination and low photocurrent in solar cells [12]. Consequently, with PCEs lagging behind those of blend devices, such approach has clearly been dismissed by the organic photovoltaic community. However, trends observed from scarce examples dealing with molecular system based on SCOSCs indicate a significant and gradual improvement in efficiencies, from less than 0.5% to more than 2.4%, as a result of a better understanding of the structure-properties-function relationships [13-17].

doi: 10.28954/2018.csq.10.001

Motivated by this challenging topic, we have recently reported the synthesis and characterization of a donor-σ-acceptor molecular dyad, consisting of a triphenylamine-based push-pull π-conjugated system linked to a fullerene (C_{60}) through a non-conjugated σ linker (**TPA-σ-C_{60}**, **Figure 1**) [18]. Beyond a modest efficiency (0.4%), we have demonstrated that such a simple architecture can lead to charge percolations within the active layer and, above all, that the simple synthetic strategy/methodology implemented in this study can be easily extended to other building blocks with different electrochemical and optical properties.

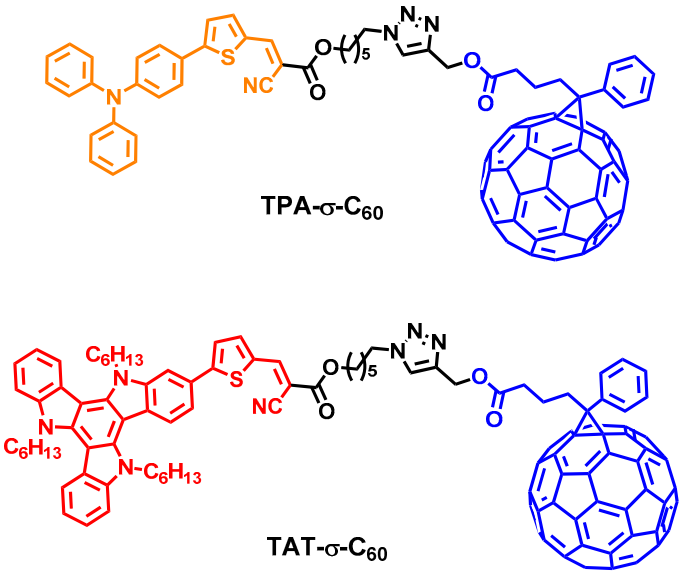

Figure 1. Illustration of the molecular dyads **TPA-σ-C_{60}** and **TAT-σ-C_{60}**

To improve the photovoltaic efficiencies, the effect of substituting the triphenylamine electron-rich block by a triazatruxene moiety is evaluated herein (**TAT-σ-C_{60}**, **Figure 1**). Indeed, though barely used in OPV [19-21], mainly as end-capping moiety, triazatruxene has already shown unique properties owing to a perfectly flat and symmetrical π-conjugated core and tunable solubility through easy modulation of the side chains on the indole units.

II. Results and Discussion

The synthetic protocol for the preparation of the molecular dyad **TAT-σ-C_{60}** is depicted in **Scheme 1**.
The N-hexyl substituted triazatruxene **TAT**, synthesized according to reported procedures [19], was first brominated in the presence of N-bromosuccinimide, and the thiophene unit was incorporated *via* reaction with tributyl(thiophen-2-yl)stannane under Stille pallado-catalyzed conditions. The resulting compound (**TAT-T**) was functionalized with a formyl moiety, which was subjected to a Knoevenagel condensation with the CH_2-activated 6-azidohexyl-2-cyanoacetate, affording the azido-functionalized push-pull molecule **TAT-σ-N_3**. Reaction of **TAT-σ-N_3** with the [6,6]-phenyl-C_{61} butyric acid propargyl ester **C_{60}-A** *via* a copper-catalyzed 1,3-dipolar Huisgen cyclo-addition finally, led to the target **TAT-σ-C_{60}** dyad.
The optical signature of the dyad, recorded in diluted dichloromethane solutions, corresponds to the superimposition of both constituents, namely the **TAT-σ-N_3** and the fullerene derivative **C_{60}-A**, confirming the weak electronic coupling between these two entities in the ground state (**Figure 2**).
According to time-dependent density-functional theory (TD-DFT) calculations (see Supporting Information), the broad band centered around 500 nm can be attributed to an internal charge transfer (ICT) from the electron-rich triazatruxene moiety to the electron-withdrawing cyanoacrylate group, thus highlighting the strong push-pull behavior of the donor part of the dyad (**Figure 3**).

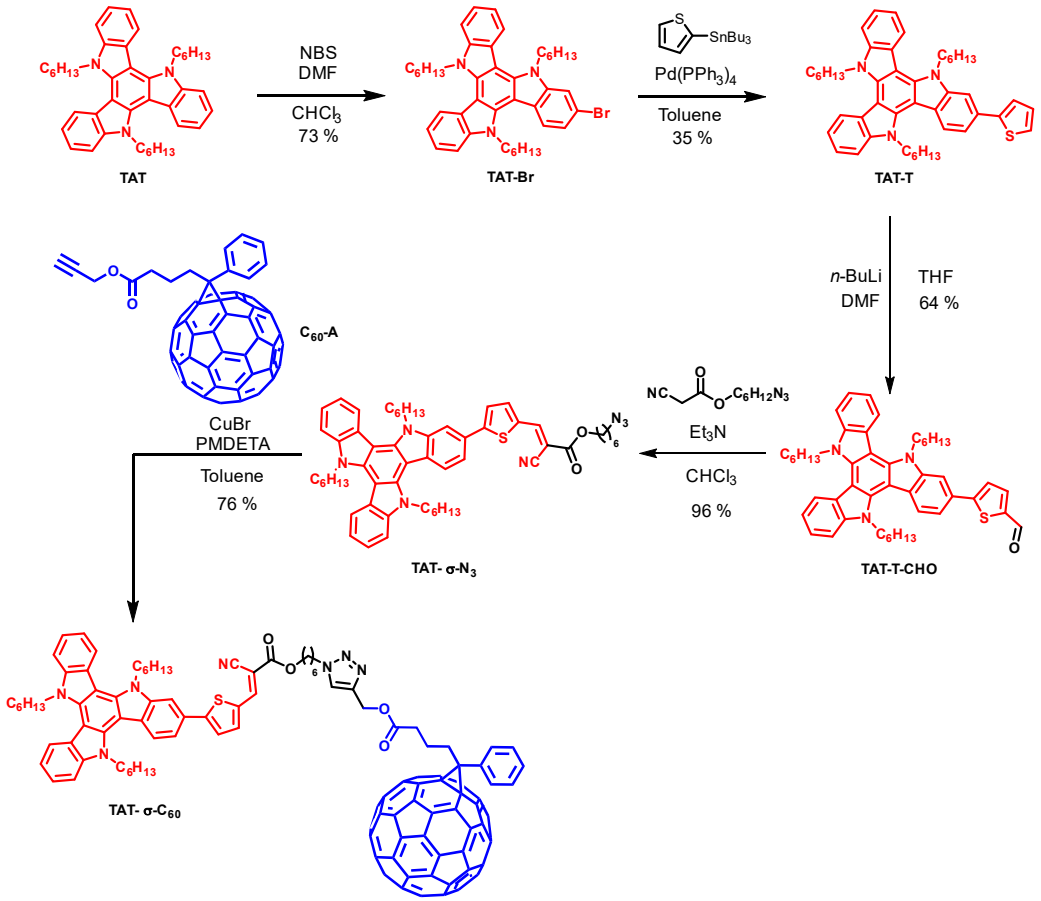

Scheme 1. Synthesis of the molecular dyad **TAT-σ-C$_{60}$**

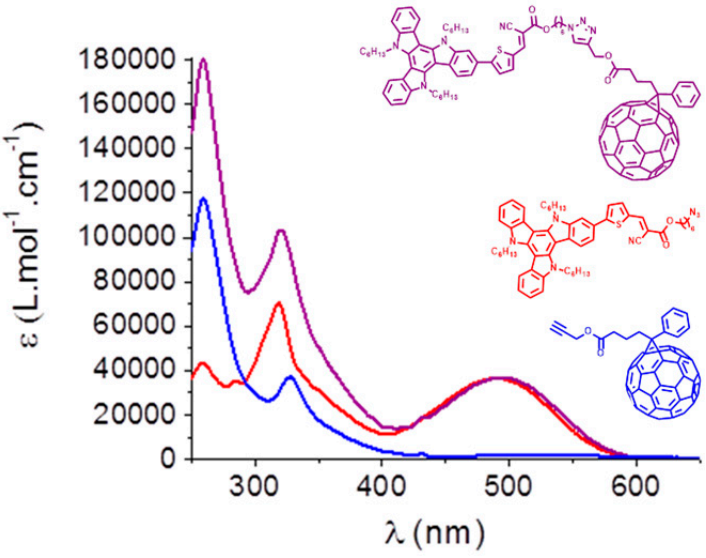

Figure 2. UV-Vis absorption spectra of **TAT-σ-C$_{60}$** (purple), **TAT-σ-N$_3$** (red), and **C$_{60}$-A** (blue) recorded in diluted CH_2Cl_2 solutions (*ca* 1 x 10^{-5} M).

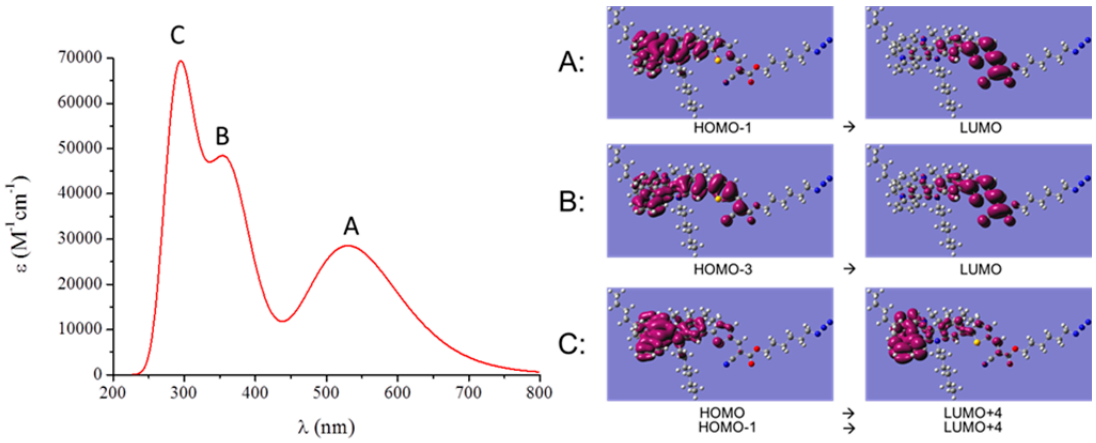

Figure 3. Theoretical simulated spectrrum of **TAT-σ-N$_3$** in dichloromethane (left) and corresponding electronic transitions (right).

The cyclic voltammogram of the dyad **TAT-σ-C$_{60}$**, performed in dichloromethane with Bu_4NPF_6 as the supporting electrolyte and exhibiting reversible oxidation and reduction waves, corresponds to the superimposition of both the donor and the acceptor moieties contributions (**Figure 4**).

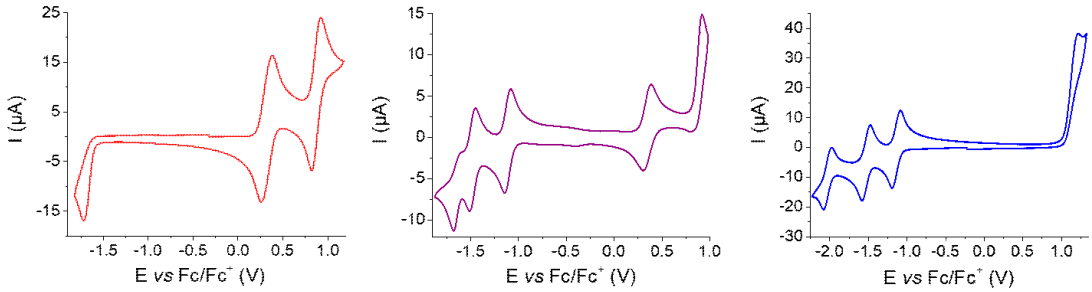

Figure 4. Cyclic voltammograms of **TAT-σ-N$_3$** (red), **TAT-σ-C$_{60}$** (purple), and the **PC$_{61}$BM** as a reference fullerene (blue) in 0.1 M Bu_4NPF_6/CH_2Cl_2, scan rate 100 mV s^{-1}, Pt working and counter electrode.

In accordance with the electrochemical signature of **TAT-σ-N$_3$**, a first reversible one-electron oxidation wave, assigned to the formation of the stable radical cation of the triazatruxene push-pull block, was recorded for **TAT-σ-C$_{60}$**. In the negative region, the two first successive reversible reduction waves can be attributed to the step-by-step, one-electron reduction of the fullerene moiety, as deduced from the cyclic voltammogram of **PC$_{61}$BM**. Finally, the third irreversible reduction process corresponds to the formation of a radical-anion on the push-pull system, once again in agreement with the pattern recorded for **TAT-σ-N$_3$** (**Table 1** and **S10**).

Table 1. Electrochemical data. V *vs* Fc+/Fc. *irreversible process. a) E_{HOMO} (eV) = − (Onset$_{ox}$ + 5.1), E_{LUMO} (eV) = − (Onset$_{red}$ + 5.1) [22].

Compound	E_{pc}^1 (V)	E_{pc}^2 (V)	E_{pc}^3 (V)	E_{pa}^1 (V)	E_{pa}^2 (V)	HOMO (eV)[a)]	LUMO (eV)[a)]
PC$_{61}$BM	-1.17	-1.56	-2.06	1.21*	-	-6.15	-4.02
TAT-σ-N	-1.71*	-	-	0.41	0.92	-5.33	-3.49
TAT-σ-C$_{60}$	-1.15	-1.51	-1.68*	0.38	0.92	-5.37	-4.05

Frontier molecular orbitals, either simulated by quantum chemistry (see Supporting Information) or estimated from the onset potentials of the oxidation and reduction processes, show favorable matching between the donor (**TAT-σ-N$_3$**) and the fullerene-based acceptor, a prerequisite for an efficient photo induced electron transfer (**Figure 4** and **Table 1**).

To evaluate the utility of the dyad as single photoactive material for organic solar cells, devices with an architecture indium tin oxide (ITO)/poly(3,4-ethylenedioxythiophene): polystyrene sulfonic acid (PEDOT:PSS)/**TAT-σ-C$_{60}$**/Al were fabricated and tested. Owing to its good solubility, different processing solvents, namely 2-methyltetrahydrofuran (MeTHF), chlorobenzene (CB) and chloroform (CF) were used to solubilize **TAT-σ-C$_{60}$**. It turns out that in the same conditions of concentration and deposition spin-speed, *i.e.*, 10 mg mL^{-1} and 4000 rpm respectively, the best quality films, and therefore best efficiencies, were obtained from chloroform solutions (**Table S1**). Power conversion efficiencies of *ca* 0.41 %, 0.22% and 0.01% were indeed obtained when the dyad is processed with CF, the CB and the MeTHF respectively.

To gain further insights, the corresponding nano-scale morphologies were investigated by atomic-force microscopy (AFM). As shown in **Figure 5**, both chloroform (CF) and chlorobenzene (CB) processed active layers showing small and homogenous nanodomains. However, with CB, a broad number of large size defects (white spots) are noticed, which are detrimental to the device performance. On the other hand, the surface topography of the active layer spun cast from the MeTHF solution reveals a quite different organization with villi-like microscopic patterns characterized by a roughness of *ca* 21 nm *vs.* 0.7 nm for the other two films (not taking into account the large defects, see Supporting Information).

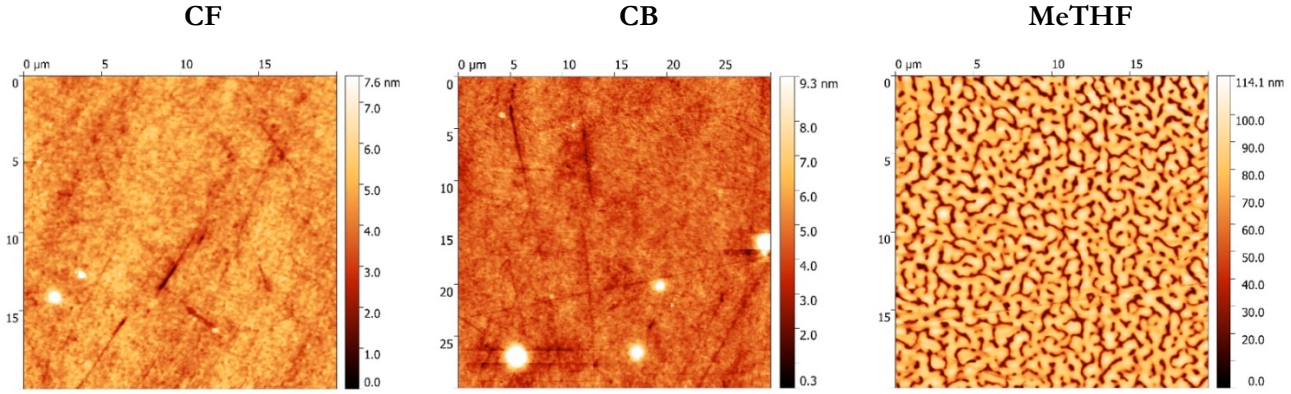

Figure 5. Surface topography images of the different active layers probed by atomic-force microscopy.

To optimize the efficiencies, the thickness dependence of the chloroform-processed active layer was then investigated, revealing an optimum around 80 nm associated to a maximum PCE of *ca* 0.56 % (**Table 2**).

Table 2. Photovoltaic data obtained with active layers of different thicknesses

Thickness (nm)	Voc (V)	Jsc (mA·cm^{-1})	FF (%)	PCE (%)
50	0.87	1.70	31.3	0.47
80	0.89	2.05	30.7	0.56
95	0.88	1.96	28.6	0.49
110	0.88	1.57	26.7	0.37
120	0.87	1.57	27.0	0.37

The corresponding current density-voltage (J-V) characteristic and the external quantum-efficiency (EQE) spectrum, performed under monochromatic irradiation, are plotted in **Figure 6**.

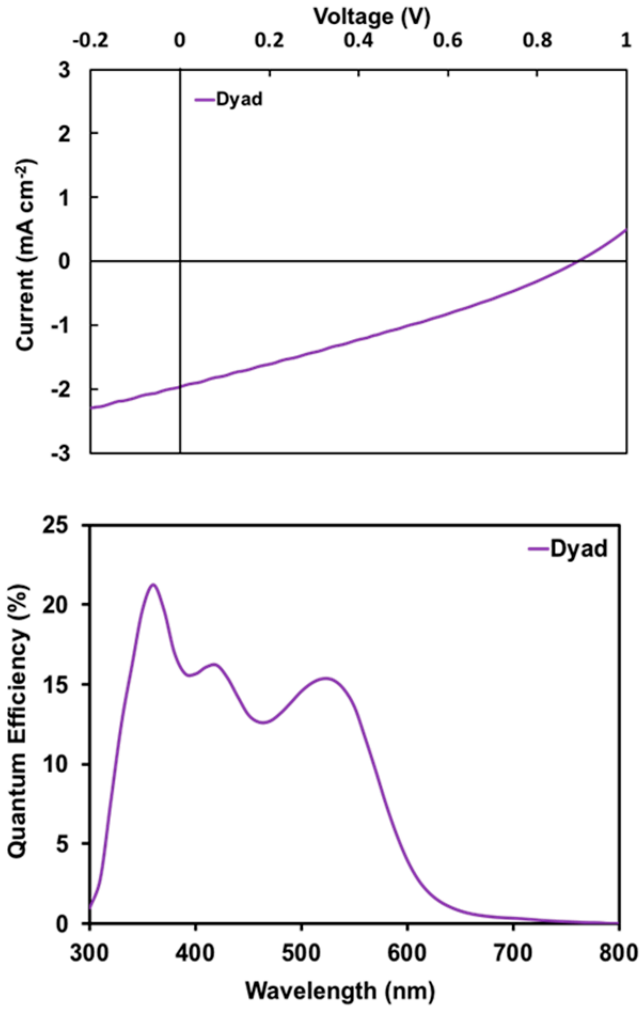

Figure 6. Top: J-V characteristics measured under AM 1.5 simulated solar light illumination (100 mW·cm^{-2}) and bottom: external-quantum efficiency spectrum of the best SCOSC based on **TAT-σ-C$_{60}$**.

In agreement with the UV-Vis experiments, the two bands at 520 nm and 420 nm can be attributed to the contribution of the TAT-based push-pull donor, while the third one, found at 360 nm, corresponds to the photon-to-current conversion of the fullerene derivative.

III. Conclusions

The synthesis of an original donor-acceptor molecular dyad and its use as electroactive material for single-component organic solar cells are demonstrated herein. Power conversion efficiencies of *ca* 0.6% were indeed measured in basic and simple devices. In addition, it is noteworthy that active layers thicker than a hundred nanometers still generate a photo-current. Although modest and still far from those of well performing bulk heterojunction blend devices, these promising results highlight the potential of such triazatruxene-based dyad to convert light into electricity, and hopefully, will contribute to a continuing surge of interest in this understudied area, namely the single-component organic photovoltaics.

IV. Additional Information

Supporting information is available online. Correspondence and requests for materials should be addressed to the corresponding author.

V. Materials and Methods

General

Ground-state DFT geometry optimizations and TD-DFT single-point calculations were carried out using GAUSSIAN 16 [23] suite package. 6-31G** basis sets were chosen for all the atomic species. The optimally-tuned ωB97X-D [24] exchange-correlation energy functional was used throughout the simulations. In order to take into account solvation effects in the reproduction of the absorption spectra, solvent dichloromethane molecules were treated as a polarizable continuum (PCM).
All reagents and chemicals from commercial sources were used without further purification. Solvents were dried and purified using standard techniques. Column chromatography was performed with analytical-grade solvents using Aldrich silica gel (technical grade, pore size 60 Å, 230-400 mesh particle size). Flexible plates ALUGRAM® Xtra SIL G UV254 from MACHEREY-NAGEL were used for TLC. Compounds were detected by UV irradiation (Bioblock Scientific) or staining with iodine, unless otherwise stated. NMR spectra were recorded with a Bruker AVANCE III 300 (^{1}H, 300 MHz and ^{13}C, 75 MHz) and a Bruker AVANCE DRX 500 (^{1}H, 500 MHz and ^{13}C, 125 MHz). Chemical shifts are given in ppm relative to tetramethylsilane (TMS) and the coupling constants J in Hz. Residual non-deuterated solvent was used as an internal standard. UV-Vis absorption spectra were recorded at room temperature on a Perkin Elmer Lambda 950 spectrometer or with a Shimadzu UV-1800. Matrix Assisted Laser Desorption/Ionization was performed on MALDI-TOF MS BIFLEX III Bruker Daltonics spectrometer using dithranol, DCTB or α-terthiophene as matrix. Cyclic voltammetry was performed using a Biologic SP-150 potentiostat with positive feedback compensation in dichloromethane solutions purchased from Carlo Erba (HPLC grade). Tetrabutylammonium hexafluorophosphate (0.1 M as supporting electrolyte) was purchased from Sigma-Aldrich and recrystallized prior to use. Experiments were carried out under an inert atmosphere (Ar) using a glovebox, by scanning the negative potential first, in a one-compartment cell equipped with a platinum working microelectrode (Ø = 2 mm) and a platinum wire as counter electrode. A silver wire immersed in 0.10 M Bu_4NPF_6/CH_2Cl_2 was used as pseudo-reference electrode and checked against the ferrocene/ferrocenium couple (Fc/Fc^+) before and after each experiment. Atomic-force microscopy (AFM) experiments were performed using the Nano-Observer device from CS Instrument. The topographic images were obtained at room temperature in tapping mode. Images were processed with the Gwyddion free SPM data analysis software.
6-Azidohexyl-2-cyanoacetate and [6,6]-phenyl-C_{61} butyric acid propargyl ester C_{60}-A were prepared according to the literature [18].

Synthesis of Compounds

TAT-Br (3-Bromo-5,10,15-trihexyl-10,15-dihydro-5H-diindolo[3,2-a:3',2'-c]carbazole): A solution of NBS (134 mg, 0.753 mmol) in DMF (7 mL) was added dropwise to a stirred mixture of **TAT** (500 mg, 0.836 mmol) in $CHCl_3$ (15 mL) at 0 °C. The resulting mixture was slowly warmed up to room temperature and stirred for an additional hour before being poured into water. The organic phase was extracted, dried over Na_2SO_4 and concentrated under vacuum. The crude product was purified by column chromatography on silica gel (eluent: Petroleum ether/Toluene 95/5 v/v) to afford **TAT-Br** (415 mg, 0.613 mmol, 73.3 %) as a white solid. ^{1}H NMR (300 MHz, $CDCl_3$): δ 8.26 (m, 2H), 8.09 (d, J = 8.6 Hz, 1H), 7.73 (d, J = 1.7 Hz, 1H), 7.63 (dd, J = 7.7, 2.6 Hz, 2H), 7.52 – 7.29 (m, 5H), 4.95 – 4.77 (m, 6H), 2.06 – 1.85 (m, 6H), 1.27 (s, 18H), 0.85 – 0.75 (m, 9H).

TAT-T (5,10,15-Trihexyl-3-(thiophen-2-yl)-10,15-dihydro-5H-diindolo[3,2-a:3',2'-c]carbazole): **TAT-Br** (400 mg, 0.591 mmol) and $Pd(PPh_3)_4$ (41 mg, 0.035 mmol) were combined in a dry Schlenk flask and purged several time by argon-vacuum cycles. Then, a freshly prepared tributyl(thiophen-2-yl)stannane (276 mg, 0.236 mL, 0.740 mmol) solution in degassed toluene (40 mL) was added and the reaction

mixture was stirred at 80 °C overnight. Upon cooling to room temperature, water was added (40 mL) and the organic phase was separated. The aqueous phase was extracted with DCM. The combined organic phases were washed over brine, dried with $MgSO_4$ and concentrated under vacuum. The crude was finally purified by column chromatography on silica gel (eluent: DCM/ PE 2/8 v/v) yielding **TAT-T** as a pale yellow solid (140 mg, 0.206 mmol, 34.8 %). ^{1}H NMR (300 MHz, $CDCl_3$): δ 8.29 (d, J = 8.0 Hz, 2H), 8.25 (d, J = 8.5 Hz, 1H), 7.83 (bs, 1H), 7.62 (m, J = 9.2 Hz, 2H + 1H), 7.46 (m, J = 7.5 Hz, 2H + 1H), 7.39 – 7.30 (m, 1H + 2H), 7.17 (dd, J = 4.8, 3.7 Hz, 1H), 4.99 – 4.86 (m, 6H), 2.08 – 1.91 (m, 6H), 1.26 (s, 18H), 0.87 – 0.77 (m, 9H).
^{13}C NMR (76 MHz, $CDCl_3$): δ 145.86, 141.64, 141.24, 141.13, 139.66, 139.16, 138.75, 129.29, 128.24, 124.36, 123.58, 123.24, 122.94, 122.77, 121.87, 121.69, 119.87, 118.45, 110.70, 110.62, 107.99, 103.52, 103.41, 103.35, 47.22, 47.12, 31.60, 31.57, 31.51, 29.95, 29.91, 29.82, 26.52, 26.50, 26.45, 22.62, 14.04.

TAT-CHO (5-(5,10,15-Trihexyl-10,15-dihydro-5H-diindolo[3,2-a:3',2'-c]carbazol-3-yl)thiophene-2-carbaldehyde): A solution of n-BuLi 1.6 M in hexanes (165 µL, 0.265 mmol) was added dropwise at -78 °C to a stirred solution of **TAT-T** (120 mg, 0.176 mmol) solubilized in 15 mL of dried THF. The mixture was stirred for 30 min at this temperature before adding DMF (26 mg, 27 µL, 0.353 mmol). The resulting mixture was stirred and allowed to warm up to room temperature overnight. The reaction was quenched with water, extracted with DCM, washed with brine, dried over $MgSO_4$ and concentrated under vacuum. The crude product was purified by column chromatography on silica gel (eluent: DCM) affording **TAT-CHO** (80 mg, 0.113 mmol, 64 %) as an orange solid. ^{1}H NMR (300 MHz, $CDCl_3$): δ 9.89 (s, 1H), 8.23 (d, *J* = 8.1 Hz, 1H), 8.19 (d, *J* = 8.2 Hz, 1H), 8.06 (d, J = 8.5 Hz, 1H), 7.72 (d, J = 4.0 Hz, 1H), 7.70 (d, J = 1.4 Hz, 1H), 7.58 (t, J = 8.2 Hz, 2H), 7.52 – 7.43 (m, 1H + 2H), 7.42 (d, J = 4.0 Hz, 1H), 7.34 (t, J = 7.5 Hz, 2H), 4.87 – 4.63 (m, 6H), 1.96 (d, J = 19.4 Hz, 6H), 1.38 – 1.13 (m, 18H), 0.89 – 0.78 (m, 9H).

TAT-σ-N_3: To a stirred solution of **TAT-CHO** (80 mg, 0.113 mmol) and 6-Azidohexyl-2-cyanoacetate (36 mg, 0.170 mmol) in $CHCl_3$ (15 mL) were added 2-3 drops of Et_3N. The reaction mixture was refluxed under argon for 3 days. Then, the solvent was removed under vacuum and the residue was purified by column chromatography on silica gel (eluent: DCM) affording **TAT-σ-N_3** as a red solid (98 mg, 0.109 mmol, 96.3 %). ^{1}H NMR (300 MHz, $CDCl_3$): δ 8.33 – 8.30 (m, 1H), 8.30 – 8.21 (m, 3H), 7.86 (d, J = 1.2 Hz, 1H), 7.80 (d, J = 4.1 Hz, 1H), 7.67 – 7.60 (m, 3H), 7.54 (d, J = 4.0 Hz, 1H), 7.51 – 7.43 (m, 2H), 7.40 – 7.31 (m, 2H), 5.00 – 4.81 (m, 6H), 4.32 (t, J = 6.6 Hz, 2H), 3.31 (t, J = 6.8 Hz, 2H), 1.99 (s, 6H), 1.87 – 1.74 (m, 2H), 1.72 – 1.60 (m, 2H), 1.52 – 1.40 (m, 4H), 1.34 – 1.16 (m, 18H), 0.84 – 0.75 (m, 9H). ^{13}C NMR (76 MHz, $CDCl_3$): δ 163.50, 156.77, 146.80, 141.33, 141.12, 141.01, 140.28, 139.74, 139.60, 138.58, 134.33, 127.07, 125.01, 123.91, 123.37, 123.13, 121.97, 121.71, 121.69, 120.09, 120.00, 118.73, 116.47, 110.76, 110.70, 108.27, 103.67, 103.29, 103.28, 96.79, 66.32, 51.49, 47.21, 31.59, 31.55, 31.45, 29.95, 29.83, 28.90, 28.60, 26.52, 26.36, 25.64, 22.62, 22.53, 14.10, 14.06, 14.03. HRMS (FAB): calculated for $C_{56}H_{65}N_7O_2S$: 899.49, found: 899.4908

TAT-σ-C_{60}: Five drops of *N,N,N′,N″,N″*-pentamethyldiethylenetriamine (PMDETA) dispersed in HPLC grade toluene (50 mL) were degassed three times via the "freeze, pump and thaw" technic. This solution was transferred using a cannula into a schlenk flask containing **C_{60}-A** (68 mg, 0.073 mmol), CuBr (5 mg) and **TAT-σ-N_3** (60 mg, 0.067 mmol) under an argon atmosphere. The reaction mixture was protected from light and stirred for one night. The solvent was then removed under vacuum and the residue was purified by chromatography on silica gel using a mixture of dichloromethane and ethyl acetate as eluent (from 100:0 v/v to 90:10 v/v). The resulting solid was further purified by dissolution in dichloromethane and subsequent precipitation with pentane to afford the pure expected **TAT-σ-C_{60}** (93 mg, 0.051 mmol, 76 %) as a brown red powder. ^{1}H NMR (499 MHz, $CDCl_3$): δ 8.33 (s, 1H), 8.29 – 8.22 (m, 3H), 7.87 (d, J = 6.9 Hz, 3H), 7.81 (d, J = 3.8 Hz, 1H), 7.68 – 7.60 (m, 4H), 7.57 – 7.42 (m, 6H), 7.39 – 7.33 (m, 2H), 5.24 (s, 2H), 5.01 – 4.84 (m, 6H), 4.38 (t, J = 7.2 Hz, 2H), 4.31 (t, J = 6.3 Hz, 2H), 2.91 – 2.80 (m, 2H), 2.56 (s, 2H), 2.24 – 2.12 (m, 2H), 2.06 – 1.89 (m, 8H), 1.82 – 1.72 (m, 2H), 1.54 – 1.47 (m, 2H), 1.47 – 1.38 (m, 2H), 1.37 – 1.31 (m, 4H), 1.30 – 1.15 (m, 14H), 0.82 (t, J = 6.6 Hz, 6H), 0.77 (t, J = 7.0 Hz, 3H). ^{13}C NMR (126 MHz, $CDCl_3$): δ 173.08, 163.45, 156.95, 148.85, 147.83, 146.89, 145.88, 145.24, 145.20, 145.18, 145.11, 145.08, 144.83, 144.78, 144.73, 144.69, 144.54, 144.46, 144.07, 143.81, 143.77, 143.16, 143.06, 143.02, 142.95, 142.25, 142.22, 142.16, 142.12, 141.41, 141.15, 141.04, 140.80, 140.37, 139.90, 139.65, 138.64, 138.09, 137.63, 136.85, 134.37, 132.22, 128.57, 128.37, 127.07, 125.15, 123.99, 123.82, 123.44, 123.17, 122.06, 121.75, 120.13, 120.05, 118.82, 116.53, 110.75,

108.36, 103.81, 103.40, 96.72, 79.92, 66.22, 57.97, 51.88, 50.38, 47.25, 34.05, 33.75, 31.61, 31.58, 31.47, 30.28, 30.00, 29.86, 28.41, 26.55, 26.51, 26.40, 26.21, 25.60, 22.63, 22.55, 22.36, 14.11, 14.07, 14.04. HRMS (FAB): calculated for $C_{130}H_{79}N_7O_4S$: 1833.59, found: 1833.5903

Device fabrication and testing: Pre-patterned indium-tin oxide coated glass slides of 24 x 25 x 1.1 mm^3 with a sheet resistance of RS = 7 Ω/sq were purchased from Visiontek Systems. The substrates were washed by successive ultrasonic baths, namely diluted Deconex® 12 PA-x solution (2% in water), acetone and isopropanol for 15 min each. Once dried under a stream of air, UV-ozone plasma treatment (Ossila UV/Ozone cleaner E511) was performed for 15 min. A filtered aqueous solution of poly(3,4-ethylenedioxy-thiophene)-poly(styrenesulfonate) (PEDOT:PSS; Ossila Al 4083) through a 0.45 µm RC membrane (Minisart® RC 15) was spun-cast onto the ITO surface at 5000 rpm for 40 s before being baked at 120 °C for 30 min. The dyad **TAT-σ-C_{60}** was then spun-cast and devices were completed by the thermal deposition of aluminum (100 nm) at a pressure of 1.5 x 10^{-5} Torr through a shadow mask defining six cells of 27 mm^2 each (13.5 mm x 2 mm). J-V curves were recorded in the dark and under illumination using a Keithley 236 source-measure unit and a home-made acquisition program. The light source is an AM1.5 Solar Constant 575 PV simulator (Steuernagel Lichttecknik, equipped with a metal halogen lamp, 100 $mW \cdot cm^{-2}$). The light intensity was measured by a broad-band power meter (13PEM001, Melles Griot). EQE were performed under ambient atmosphere using a halogen lamp (Osram) with an Action Spectra Pro 150 monochromator, a lock-in amplifier (Perkin-Elmer 7225) and a S2281 photodiode (Hamamatsu).

VI. Conflict of Interests

The authors declare there are no conflicts of interests.

VII. Acknowledgements

The *Région Pays de la Loire* and the RFI LUMOMAT are thanked for the PhD grant of A. L. and the funding of the SAMOA project (*Etoile Montante 2017*). Authors thank the MATRIX SFR of the University of Angers and more precisely the ASTRAL and CARMA platforms for the characterization of organic compounds and device preparation/characterization respectively. G. L. thanks the European Union's Horizon 2020 research and innovation program under Marie Sklodowska Curie Grant agreement No.722651 (SEPOMO). The work in the Laboratory for Chemistry of Novel Materials was supported by the Consortium des Équipements de Calcul Intensif (CÉCI), funded by the Fonds de la Recherche Scientifiques de Belgique (F.R.S.- FNRS) under Grant No. 2.5020.11, as well as the Tier-1 supercomputer of the Fédération Wallonie-Bruxelles, infrastructure funded by the Walloon Region under Grant Agreement No. 1117545. D.B. is a FNRS Research Director .G. C. W. and S. V. D thank the University of Calgary and the Canadian Foundation for Innovation for salary and solar cell equipment support, respectively.

VIII. References

[1] Meng, L., Zhang, Y.; Wan, X., Li, C., Zhang, X., Wang, Y., Ke, X., Xiao, Z., Ding, L., Xia, R., Yip, H.-L., Cao, Y., Chen, Y., *Science*, **2018**, 1094-1098.

[2] Che X., Li, Y., Qu Y., Forrest, S. R., *Nature Energy*, **2018**, *3*, 422-427.

[3] Zhao, W., Li, S., Yao, H., Zhang, S., Zhang, Y., Yang B., Hou, J., *J. Am. Chem. Soc.*, **2017**, *139*, 7148-7151.

[4] Antohe, S., Iftimie, S., Hrostea, L., Antohe V. A., Girtan, M., *Thin Solid Films*, **2017**, *642*, 219-231.

[5] Beaujuge P. M., Fréchet, J. M. J., *J. Am. Chem. Soc.*, **2011**, *133*, 20009-20029.

[6] Warnan, J., El Labban, A., Cabanetos, C., Hoke, E. T., Shukla, P. K., Risko, C., Brédas, J.-L., McGehee M. D., Beaujuge, P. M., *Chem. Mater.*, **2014**, *26*, 2299-2306.

[7] Graham, K. R., Cabanetos, C., Jahnke, J. P., Idso, M. N., El Labban, A., Ngongang Ndjawa, G. O., Heumueller, T., Vandewal, K., Salleo, A., Chmelka, B. F., Amassian, A., Beaujuge P. M., McGehee, M. D., , *J. Am. Chem. Soc.*, **2014**, *136,* 9608-9618.

[8] Dang, M. T., Wantz, G., Bejbouji, H., Urien, M., Dautel, O. J., Vignau L., Hirsch, L., *Solar Energy Materials and Solar Cells*, **2011**, *95*, 3408-3418.

[9] Dang, M. T., Hirsch, L., Wantz G., Wuest J. D., *Chem. Rev.*, **2013**, *113,* 3734-3765.

[10] Segura, J. L., N. Martín, N., Guldi, *D.* M., *Chem. Soc. Rev.,* **2005**, *34,* 31-47.

[11] Nierengarten, J.-F., Eckert, J.-F., Nicoud, J.-F., Ouali, L., Krasnikov V., Hadziioannou, G., *Chem. Commun.*, **1999**, *7,* 617-618.

[12] Roncali, J., *Adv. Energy Mater.*, **2011**, *1*, 147-160.

[13] Chen, T. L., Zhang, Y., Smith, P., Tamayo, A., Liu Y., Ma, B., *ACS Appl. Mater. Inter.*, **2011**, *3,* 2275-2280.

[14] Narayanaswamy, K., Venkateswararao, A., Nagarjuna, P., Bishnoi, S., Gupta, V., Chand, S., Singh, S. P., *Angew. Chem. Int. Ed.*, **2016**, *55,* 12334-12337.

[15] Nguyen, T. L., Lee, T. H., Gautam, B., Park, S. Y., Gundogdu, K., Kim J. Y., Woo, H. Y., *Adv. Func. Mater.*, **2017**, *27*, 1702474.

[16] Nishizawa, T., Lim, H. K., Tajima K., Hashimoto, K., *Chem. Commun.*, **2009**, *18*, 2469-2471.

[17] Izawa, S., Hashimoto, K., Tajima, K., *Phys. Chem. Chem. Phys.*, **2012**, *14*, 16138-16142.

[18] Labrunie A., Gorenflot J., Babics M., Alévêque O., Dabos-Seignon S., Balawi A. H., Kan Z., Wohlfahrt M., Levillain E., Hudhomme P., Beaujuge P. M., Laquai F., Cabanetos C., Blanchard P., *Chem. Mater.*, **2018**, *30,* 3474-3485.

[19] Bura, T., Leclerc, N., Bechara, R., Lévêque, P., Heiser T., Ziessel, R., *Adv. Energy Mater.*, **2013**, *3*, 1118-1124.

[20] Bura, T., Leclerc, N., Fall, S., Lévêque, P., Heiser T., Ziessel, R., *Org. Lett.*, **2011**, *13,* 6030-6033.

[21] Bulut, I., Lévêque, P., Heinrich, B., Heiser, T., Bechara, R., Zimmermann, N., Méry, S., Ziessel, R., Leclerc, N., *J. Mater. Chem. A*, **2015**, *3*, 6620-6628.

[22] Cardona, C. M., Li, W., Kaifer, A. E., Stockdale D., Bazan, G. C., *Adv. Mater.*, **2011**, *23,* 2367-2371.

[23] Frisch, M. J., Trucks, G. W., Schlegel, H. B., Scuseria, G. E., Robb, M. A., Cheeseman, J. R., Scalmani, G., Barone, V., Petersson, G. A., Nakatsuji, H., Li, X., Caricato, M., Marenich, A. V., Bloino, J., Janesko, B. G., Gomperts, R., Mennucci, B., Hratchian, H. P., Ortiz, J. V., Izmaylov, A. F., Sonnenberg, J. L., Williams-Young, D., , Ding, F., Lipparini, F., Egidi, F., Goings, J., Peng, B., Petrone, A., Henderson, T., Ranasinghe, D., Zakrzewski, V. G., Gao, J., Rega, N., Zheng, G., Liang, W., Hada, M., Ehara, M., Toyota, K., Fukuda, R., Hasegawa, J., Ishida, M., Nakajima, T., Honda, Y., Kitao, O., Nakai, H., Vreven, T., Throssell, K., Montgomery Jr., J. A., Peralta, J. E., Ogliaro, F., Bearpark, M. J., Heyd, J. J., Brothers, E. N., Kudin, K. N., Staroverov, V. N., Keith, T. A., Kobayashi, R., Normand, J., Raghavachari, K., Rendell,A. P., Burant, J. C., Iyengar, S. S., Tomasi, J., Cossi, M., Millam, J. M., Klene, M., Adamo, C., Cammi, R., Ochterski, J. W., Martin, R. L., Morokuma, K., Farkas, O., Foresman J. B., Fox, D. J., *Gaussian 16 Rev. B.01*. **2016**, Wallingford, CT.

[24] Chai, J.-D., Head-Gordon, M., *Phys. Chem. Chem. Phys.,* **2008**, *10*, 6615-6620.

Received: 30 August 2018
Accepted: 17 October 2018
Published online: 31 October 2018

ORCID ID for authors
Clément Cabanetos: 0000-0003-3781-887X
Phillippe Blanchard: 0000-0002-9408-8108
Gregory Welch: 0000-0002-3768-937X
Giacomo Londi: 0000-0001-7777-9161
Sergey Dayneko: 0000-0002-0604-6099
Sylvie Dabos-Seignon: 0000-0002-7900-6354